Determination of a non-perturbed reference for a new version of the disturbance ionosphere index

Giorgio Arlan da Silva Picanço (giorgio.picanco@inpe.br)
Instituto Nacional de Pesquisas Espaciais https://orcid.org/0000-0003-3926-396X

Clezio Marcos Denardini
Instituto Nacional de Pesquisas Espaciais

Paulo Alexandre Bronzato Nogueira
Federal Institute of Education, Science and Technology of São Paulo

Paulo França Barbosa-Neto
Instituto Nacional de Pesquisas Espaciais

Láysa Cristina Araújo Resende
Instituto Nacional de Pesquisas Espaciais

Carolina de Sousa do Carmo
Instituto Nacional de Pesquisas Espaciais

Esmeralda Romero-Hernandez
Universidad Autonoma de Nuevo Leon

Sony Su Chen
Instituto Nacional de Pesquisas Espaciais

Juliano Moro
Instituto Nacional de Pesquisas Espaciais

Regia Pereira da Silva
Instituto Nacional de Pesquisas Espaciais

Full paper

Keywords: TEC, DIX, Ionospheric Indices, Space Weather

Posted Date: August 6th, 2020

DOI: https://doi.org/10.21203/rs.3.rs-51725/v1

Determination of a non-perturbed reference for a new version of the disturbance ionosphere index

Author #1: Giorgio Arlan da Silva Picanço*, National Institute for Space Research, 12227-010, São José dos Campos - SP, Brazil, giorgio.picanco@inpe.br

Author #2: Clezio Marcos Denardini, National Institute for Space Research, 12227-010, São José dos Campos - SP, Brazil, clezio.denardin@inpe.br

Author #3: Paulo Alexandre Bronzato Nogueira, Federal Institute of Education, Science and Technology of São Paulo, Jacareí - SP, Brazil, paulo.nogueira@ifsp.edu.br

Author #4: Paulo França Barbosa Neto, National Institute for Space Research, 12227-010, São José dos Campos - SP, Brazil, paulo.barbosa@inpe.br

Author #5: Láysa Cristina Araújo Resende, State Key Laboratory of Space Weather, NSSC/CAS, Beijing, China, and National Institute for Space Research, 12227-010, São José dos Campos - SP, Brazil, laysa.resende@inpe.br

Author #6: Carolina de Sousa do Carmo, National Institute for Space Research, 12227-010, São José dos Campos - SP, Brazil, carolina.carmo@inpe.br

Author #7: Esmeralda Romero Hernandez, Universidad Autónoma de Nuevo León,

Facultad de Ciencias Físico-Matemáticas, LANCE, Monterrey, Mexico,

esmeralda.romerohdz@uanl.edu.mx

Author #8: Sony Su Chen, National Institute for Space Research, 12227-010, São José dos Campos - SP, Brazil, sony.chen@inpe.br

Author #09: Juliano Moro, State Key Laboratory of Space Weather, NSSC/CAS, Beijing, China, and National Institute for Space Research, 12227-010, São José dos Campos - SP, Brazil, julianopmoro@gmail.com

Author #10: Regia Pereira da Silva, Northeast Regional Center – CRN/INPE, 59076-740, Natal – RN, Brazil, regia.pereira@inpe.br

*Corresponding author: INPE/DIDAE, Avenida dos Astronautas, 1758, Jardim da Granja, 12227-010, São José dos Campos, SP, Brazil; Tel.: +55 12 3208-7155; E-mail: giorgio.picanco@inpe.br; giorgiopicanco@gmail.com

Abstract

In the present work, we propose and evaluate a new method for the determination of a non-perturbed Total Electron Content (TEC) reference to apply it on a new version of the disturbance ionosphere index (DIX). This method is based on the calculation of a 3-hour moving average over the TEC obtained during a given reference day (named 3hMAQd method). In this context, the reference day is supposed to represent a quiet pattern considering geomagnetic and ionospheric features. To evaluate its performance, we compared the proposed method with TEC values obtained from monthly medians and the International Reference Ionosphere (IRI) model. The results are presented and discussed in terms of a dispersion coefficient between each method and the averaged TEC from the five quietest days of each month of 2015, over three Brazilian sites. Finally, we calculated the new DIX based on our proposed method and compared it with the original DIX values obtained during the extreme space weather event of St. Patrick's Day magnetic storm (17-18 March 2015). Differences between the two DIX approaches are discussed to show the improvements in new DIX due to the application of the proposed non-perturbed reference. Moreover, results showed that the quality of

the DIX calculation can be highly influenced by the non-perturbed reference determination. In this regard, the 3-hour moving average (3hMAQd) method showed to be a quite appropriate technique for the new DIX calculation, besides the 3-hour window matches with ordinary magnetic indices resolution (e.g. Kp and Ksa).

Keywords

TEC, DIX, Ionospheric Indices, Space Weather

1 Introduction

Ionospheric disturbances have a strong influence on the performance of radio-based Global Navigation Satellite System (GNSS) (e.g. GPS, GLONASS, and Galileo). These effects may include serious errors caused by rapid phase and amplitude fluctuations on transionospheric radio signals, as well as interruptions in the satellite-receiver connection due to loss of lock (Klobuchar, 1991; Jakowski et al., 2012a). In this framework, ionospheric disturbances can be defined in terms of the abnormal variations observed on values of TEC, being mainly related to phenomenon driven by solar

63 eruptive/radiative events and/or associated with dynamical processes of the Earth's
64 atmosphere (Batista et al., 1991; Sobral et al., 1997; Abdu et al., 2006; Takahashi et al.,
65 2016). Thus, the use of planetary geomagnetic indices, such as AE and Dst is still
66 insufficient to represent the local ionospheric behavior as well as to detect ionospheric
67 disturbances (Jakowski et al., 2012b). Nevertheless, many efforts have been made to
68 develop indices that better represent the ionospheric response due to external and
69 internal drivers (e.g. Coronal Mass Ejections [CMEs], solar flares, and Medium Scale
70 Travelling Ionospheric Disturbances [MSTIDs]) (Denardini et al., 2020a, 2020b;
71 Jakowski and Hoque, 2019; Resende et al., 2019).
72 Denardini et al. (2020a) present a chronological list of some of the most well-known
73 ionospheric indices as well as a basic description of its calculation methodologies.
74 These methodologies have been developed aiming to provide a quick measure of the
75 abnormal ionospheric variations (e.g. TEC gradients due to ionospheric storms). Among
76 those listed indices, some ones have been constantly used as a practical way to measure
77 ionospheric disturbances based on well-established parameters, such as TEC. Also,
78 many examples using TEC-based ionospheric indices can be found in the literature

(Gulyaeva and Stanislawska, 2008; Jakowski et al., 2006, 2012b; Sanz et al., 2014; Voeykov et al., 2018; Wilken et al., 2018). Moreover, TEC-based ionospheric indices are generally calculated from satellite data.

Starting from the concept of abnormal TEC variations, we consider that it is primarily necessary to understand what a typical TEC variation is before to define a threshold for an abnormal/disturbed behavior. With that in mind, we intend to make it clear the differences between an ionospheric background value (non-perturbed TEC reference) and a disturbed state value (variation concerning the non-perturbed reference). These two parameters have been widely used in the study of ionospheric variations with different time scales (Figueiredo et al., 2017, 2018a; Takahashi et al., 2018; Shinbori et al., 2018; Tsugawa et al., 2018). Therefore, the proper definition of a non-perturbed TEC reference is an essential matter to make sure that the index value is consistent with what happens in the ionosphere.

With the aim to express the ionosphere response due to perturbations over a given region, Jakowski et al. (2006) proposed the first formulation of a TEC-based parameter named Disturbance Ionosphere indeX (DIX), which was obtained from GNSS data.

Given this perspective, the DIX is based on the TEC variation over a background calculated from TEC monthly medians, here referred to as a 'non-perturbed reference'. The most important point of a non-perturbed reference is how well it can represent a quiet pattern just considering geomagnetic and ionospheric features. This point is essential because a non-perturbed reference must include TEC values related to the expected behavior of a given day, excluding the ionospheric disturbances contribution (considering those disturbances driven by external and/or internal sources). In this sense, an inappropriate methodology for an ionospheric index can over/underestimate the real behavior of the ionosphere by increasing/decreasing the TEC values during the non-perturbed reference calculation.

Therefore, the main aims of this study are to propose and to evaluate a new method to obtain the non-perturbed reference for a DIX formulation presented by Denardini et al. (2020a) (here referred to as "new DIX"). We also intended to study different approaches to represent the reference pattern as a function of temporal and spatial TEC variations. Therefore, we demonstrate that the proposed method leads to an acceptable reference for the new DIX by comparing it with some other methods, such as the one

111 used by Jakowski et al. (2006), and another one defined by the use of TEC data
112 obtained from the IRI model (Bilitza et al., 2017). Those comparisons were performed
113 in terms of their similarities with the averaged TEC obtained from the five
114 geomagnetically quietest days of each month of the year 2015, determined by the
115 German Research Centre for Geosciences (GFZ). Additionally, we propose a dispersion
116 coefficient to evaluate the quality of each of the methods concerning the similarity with
117 the above-mentioned 5-days average. From that analysis, we select the proper method
118 for the new DIX non-perturbed reference calculation, for three Brazilian sites during the
119 year 2015. Finally, we calculated the new DIX values by using the proposed
120 non-perturbed reference over the period around the St. Patrick's Day magnetic storm
121 (17-18 March 2015) and compared it with the DIX values obtained from the original
122 methodology towards discussing the differences between both indices. The results
123 showed that the selected method is an adequate alternative to represent the new DIX
124 non-perturbed reference.
125
126

2 Methodology

2.1 Original DIX and new DIX indices

The DIX is an ionospheric-disturbances index proposed in a first formulation by Jakowski et al. (2006) and later evolved through the modification and inclusion of various parameters (Jakowski et al., 2012a, 2012b, 2019; Wilken et al., 2018; Denardini et al., 2020a). In its first formulation, the DIX was named Regional Ionosphere Disturbances IndeX (RIDX), corresponding to a way of representing the ionospheric degree of perturbation over a given region containing *n* observations (piercing points). Basically, the RIDX is based on the deviation of TEC values from a non-perturbed reference obtained from TEC monthly medians. Thus, the index is defined in the Equation (1) (Jakowski et al., 2006):

$$\mathrm{RIDX}_{\mathrm{r}}^{\mathrm{med}} = \sqrt{\left(\frac{1}{\mathrm{N_{grp}} - 1}\right) \sum_{\mathrm{k}=1}^{\mathrm{N_{grp}}} \left(\left(\mathrm{TEC_k} - \mathrm{TEC_k^{med}}\right)/\mathrm{TEC_k^{med}}\right)^2} \quad (1)$$

where $\mathrm{TEC_k}$ is the vertical TEC value obtained for a given piercing point $k = (latitude, longitude)$, $\mathrm{TEC_k^{med}}$ is the corresponding TEC monthly median, and $\mathrm{N_{grp}}$ is the number of observation points in the region of interest.

144 In the present work, we used not an average of observation points over a region (see
145 Equation 1), but single-point vertical TEC data obtained from the TEC maps developed
146 at the "Brazilian Studies and Monitoring of Space Weather" (Embrace/INPE)
147 (Takahashi et al., 2016), which is a custom version of the earlier procedure presented by
148 Otsuka el al. (2002). Considering the use of single-point observations, we used the
149 RIDX equation modified by Denardini et al. (2020a) for only one observation point
150 (here referred to as original DIX), for comparison purposes. In this way, we compared
151 the "new DIX" values calculated using the proposed non-perturbed reference with the
152 "original DIX" values. The new DIX is defined by the Equation (2), as explained in
153 details by Denardini et al. (2020a):
154

$$\mathrm{DIX}_k(t) = \sqrt{\left(\frac{\alpha\left(\Delta TEC_k(t)/TEC_k^{Qd}(t)\right) + \Delta TEC_k(t)}{\beta}\right)^2}, \qquad (2)$$

155

156 where TEC_k is the same term described in Equation (1), TEC_k^{Qd} corresponds to the
157 non-perturbed reference value at a given time over the observation point. However,
158 TEC_k^{Qd} differs from the TEC_k^{med} since we are using the methodology proposed in this

159 study. The term $\Delta TEC_k = \left|TEC_k(t) - TEC_k^{Qd}(t)\right|$ and the coefficient α (both given in
160 TEC units) intend to improve the new DIX sensitivity to internal drivers as well as to
161 normalize its response irrespective of the local time. Finally, the coefficient β (also
162 given in TEC units) is chosen to normalize the DIX output into a scale ranging from 0
163 to 5. More details are given in Denardini et al., (2020a).
164 In view of the above, the comparison between two values derived from single piercing
165 points (original DIX and new DIX) is more appropriate for the non-perturbed reference
166 analysis since it mitigates effects due to spatial ionospheric variations. Therefore, the
167 main aim in the present work was to find an adequate methodology for representing the
168 non-perturbed reference, $\mathrm{TEC_k^{Qd}}$, as presented in the Equation (1).
169

170 **2.2 Determination of the reference day**

171 As proposed by Jakowski et al. (2006), monthly medians are a simple method to represent
172 a non-perturbed TEC reference. However, including data obtained during periods with
173 the occurrence of magnetic storms may lead the reference values to be contaminated with
174 a high-amplitude noise due to magnetic perturbation effects (e.g. positive/negative

ionospheric storms due to prompt penetration, disturbance dynamo electric fields, and thermospheric composition changes) (Kelley et al., 1979; Blanc and Richmond, 1980; Wu et al., 2004; Abdu et al., 2006, Nogueira et al., 2011, de Siqueira, 2011). Thus, we propose an alternative method to determine a non-perturbed reference for the new DIX. The method is based on the use of a centered moving average of the TEC obtained during a reference day along a period of interest of up to 15 days. This 2-week window is set to mitigate seasonal effects. In this regard, we define the reference day as the geomagnetically quietest day of the period of interest where no plasma depletions greater than 20 TEC units (TECU) along a period of 1 hour have been observed, and no spread-F over a low-latitude station has been reported. We adopt this procedure once a day considered geomagnetically quiet does not guarantee that it does not present disturbances related to sources within the ionosphere (e.g. Equatorial Plasma Bubbles [EPBs] and MSTIDs) (Takahashi et al., 2018; Figueiredo et al., 2018b). This criterion of 20 TEC units is based on our experience with EPB studies in Brazil. With this in mind, the geomagnetically quietest day is firstly selected from the list provided by GFZ Potsdam, and the presence/absence of spread-F is posteriorly confirmed by observing ionograms

191 from a low-latitude station (from 21:00 UT to 24:00 UT). In this sense, the reference day
192 is supposed to represent a quiet pattern considering geomagnetic and ionospheric
193 features.

194 An example of the method used to observe the occurrence of spread-F is presented in the
195 Figure 1, which provides a sequence of nine ionograms (virtual heights vs. reflection
196 frequencies) obtained from the ionosonde operating in Cachoeira Paulista (CPA,
197 22.67°S, 44.99ºW). These ionograms were obtained over the interval between 21:00 UT
198 and 23:30 UT on March 14, 2015. Observing the behavior of both ordinary and
199 extraordinary wave modes on the ionograms, we can clearly see that the occurrence of
200 spread-F was not reported (Abdu et al., 2009; Resende et al., 2019). Considering that the
201 daily sum of Kp is 10.67, along with no observation of TEC depletions and spread-F, we
202 are able to state that 14 March can represent a reference day. Consequently, this reference
203 gathers characteristics of a quiet pattern considering geomagnetic and ionospheric
204 features.

205

206

207 **2.3 Non-perturbed TEC reference calculation**

208 After these initial steps, the non-perturbed reference can be obtained by calculating a
209 centered moving average over the TEC data related to the above-mentioned reference
210 day. Therefore, our non-perturbed reference, MAQd, can be obtained using the
211 Equation (3):

212

213 $$\mathrm{MAQd(t)} = \frac{1}{2w+1}\sum_{\delta=-w}^{w} TEC(t+\delta) \qquad (3)$$

214

215 where $TEC(t)$ is the TEC value at a given time, t, the term δ is the lower limit of the
216 moving average time scale (given in minutes), and w is the point that should delimit
217 the sampling scale so that the non-perturbed reference value obtained has a position
218 equivalent to TEC_k on the DIX equation.

219

220 The w value is given by:

221

$$w = \begin{cases} (N-1)/2, & \text{if } N \text{ is odd} \\ (N/2)-1, & \text{if } N \text{ is even'} \end{cases} \quad (4)$$

where N is the number of samples contained in the moving average window (e.g. for 60 minutes, $N = 60$)

3 Data Set and Evaluation of the Proposed Method

To empirically evaluate the efficacy of the proposed method in representing a non-perturbed reference, we used the TEC values obtained from TEC maps at three locations of GNSS stations in Brazil (single-points): São Luís (SLZ), São José dos Campos (SJC), and Santa Maria (SMA). The geographic and geomagnetic coordinates of the locations whose data were used in this study are given in Table 1.

231 Figure 2 shows an example of the Embrace/INPE TEC map over South America
232 including the geographical locations of the three TEC single-points used in the present
233 work (SLZ, SJC, and SMA). The solid black line across the map represents the
234 magnetic equator in 2015.

235

236 Considering the Figure 2, we have chosen each of the three locations from the following
237 requirements:

238 • One site located in the neighborhood of the magnetic equator (SLZ);
239 • One site located nearby the Equatorial lonization Anomaly (EIA) southern crest
240 (SJC); and
241 • One site located south of the southern EIA crest (SMA).

242 In such a scenario, scattered locations around the EIA crest can provide different
243 viewpoints of the TEC behavior throughout the year (Takahashi et al., 2014). In this
244 way, we calculated the non-perturbed reference values for the year 2015 using the
245 proposed method. These calculations were made for the three sites within three different

246 time scales: 1 hour (1hMAQd), 3 hours (3hMAQd), and 6 hours (6hMAQd). We
247 compared the non-perturbed series (1,3 and 6h-MAQd) with the TEC monthly medians
248 and with the TEC data provided by the IRI model, for the same period and same sites,
249 aiming to determine the best methodology for the non-perturbed TEC reference. These
250 comparisons were made from the determination of a similarity parameter between each
251 method and the average of the TEC obtained during the five geomagnetically quietest
252 days of each month (here referred as to "quiet TEC"), as an attempt to correlate each
253 reference TEC values with a geomagnetically quiet reference. In this context, we
254 assume that the non-perturbed reference for the new DIX must be similar to the
255 expected TEC curve during a geomagnetically quiet day, excluding plasma bubble
256 effects (see Session 2.2).

257 To calculate the above-mentioned similarity parameter, we propose a simple and useful
258 dispersion coefficient, χ, given by the Equation (5):

259

260 $$\chi = \sqrt{(1-a)^2 + (1-r)^2} \quad (5)$$

261

where a is the slope of the linear regression between the TEC reference (MAQd, Monthly Medians or TEC-IRI) and the quiet TEC measurements, and the term r is the Pearson's correlation coefficient between the same values.

Therefore, we have a simple parameter whose value corresponds to a single dispersion coefficient. Thus, the closer to zero the χ value is, the closer the non-perturbed reference TEC values are to the quiet TEC values, attesting to the quality of the method. The opposite is also true. The higher the χ value is, the worse is the comparison with the quiet TEC.

4 Results and Discussions

4.1 Non-perturbed references variation with respect to the reference day

Here we intend to compare the different non-perturbed references with their respective reference days. In the case of the monthly medians, this comparison was performed with TEC values for the whole month of 2015. Regarding TEC-IRI values and MAQd values, the analysis considers the same reference day for the comparison.

Figure 3 displays an example of the time variation of non-perturbed TEC references

278 calculated from each of the methods as described above. In this figure, each column
279 (with different colored lines) represents the time variation for each non-perturbed
280 reference method during February 2015 (black: monthly medians, red: TEC-IRI, blue:
281 1hMAQd, orange: 3hMAQd, and green: 6hMAQd), for the three TEC sites (from the
282 upper to the bottom panels: SLZ, SJC, and SMA). The TEC from the reference day is
283 represented by the gray curves. It is emphasized that each TEC monthly median is
284 calculated from all TEC values during each month (only February in this case).
285 Therefore, the left panel also shows all TEC curves from which the monthly medians
286 curve is obtained.
287 As shown in Figure 3, the monthly medians are calculated over TEC curves presenting
288 differences from each other from 15 TECU (around 07:00 UT) to 50 TECU (around
289 18:00 UT). This feature can be seen on the SLZ monthly median, where the measured
290 TEC curve's maximum value near 18:00 UT ranges from about 55 to 75 TEC units. In
291 the SJC monthly medians, it can be seen that the maximum daily TEC values are
292 ranging from 60 to 110 TEC units. Additionally, the TEC measured at SMA presents
293 maximum values ranging from 55 to 100 TEC units. Thus, TEC curves from SLZ and

SMA show fewer amplitude variations than the SJC curves. It can also be seen a peak at 18:00 UT in the TEC measured at SJC on February 19 (yellow curve), being possibly an electric field signature during a CME-driven geomagnetic storm with ionospheric effects at low latitudes (Worku, 2019). In addition to these observations, it is reasonable to say that the calculation of a non-perturbed reference based on monthly medians can be highly influenced by TEC values obtained during days with the occurrence of storm-related ionospheric disturbances.

Figure 3 also shows that TEC-IRI values tend to be similar to those on the reference day only in the time interval between 00:00 UT to 12:00 UT but underestimate the values over SJC and SMA in the early hours. These TEC values are quite different during other times of the day. Indeed, TEC values closest to the reference day are observed in the non-perturbed references calculated using the MAQd method. In this way, it is observed that the 1hMAQd method provides a good smoothness of the reference day TEC short-term time variations.

However, looking at the 3hMAQd curve we can observe that the short-time TEC variations (less than 3 hours amplitude) are efficiently smoothed by this process. This

aspect can be clearly observed at the SJC site panel, around 18:00 UT, where the double peak in the reference day TEC is smoothed into a single one by the 3hMAQd curve. The same feature is not observed when the 1hMAQd method is used since the double peak in TEC remains present. Since the TEC amplitude has not been significantly changed in comparison to the reference day curve, such behavior is a good feature concerning the improvement of the new DIX sensitivity to short time scale ionospheric phenomena (e.g. Traveling Ionospheric Disturbances [TIDs]). As well as the 3hMAQd method, the 6hMAQd is also capable of smooth out short-term time variations. Nonetheless, the 6hMAQd tends to include significant amplitude differences in the non-perturbed reference with respect to the reference day TEC, as can be seen from the SJC and SLZ curves.

4.2 Analysis of the coefficients

Here we intend to compare the non-perturbed reference values obtained from the different methods with the quiet TEC values, which are an average of the TEC obtained during the five geomagnetically quietest days of a given month. Thus, Figure 4 displays

the scatter plots of the non-perturbed references calculated from the monthly medians (black symbols), TEC-IRI (red symbols), 1hMAQd (blue symbols), 3hMAQd (orange symbols), and 6hMAQd (green symbols) at (a) SLZ, (b) SJC , and (c) SMA versus the quiet TEC (qTEC) values obtained in February 2015, respectively.

Two features can be easily observed in Figure 4. The first one is that all non-perturbed values related to qTEC values tend to be more dispersed on the TEC site located in the EIA southern crest (SJC). This characteristic can be explained by the mechanism described in Abdu (2005), who states that due to the increase (decrease) of the eastward zonal electric field, the transport of plasma driven by the fountain effect is also intensified (decreased) causing plasma from the EIA crest to be displaced towards higher (lower) latitudes. Moreover, Abdu (2005) emphasizes the importance of the thermospheric meridional wind for the position of the EIA crest. Thus, the EIA crest behavior makes TEC at SJC to be more variable than others with respect to its day-to-day variability. The other feature is that all methods have Pearson's correlation coefficient values greater than 0.9. Thus, it is difficult to select a non-perturbed reference method for the new DIX just considering the r value. Therefore, we decided

342 to select it from the results coming from the dispersion coefficient (see Equation 5).

343 The corresponding annual averages of the dispersion coefficient values for each
344 non-perturbed reference method are listed in Table 2. It is observed that the
345 non-perturbed reference method that comes closest to qTEC is the one obtained from
346 the calculation of a 1-hour moving average over the TEC obtained during the reference
347 day (1hMAQd). The monthly medians and the 3hMAQd methods are quite similar,
348 having even equal χ-values for the SLZ site. However, it is emphasized that the
349 monthly medians may include both quiet and disturbed days in its calculation and so are
350 disregarded in the new DIX calculation (see results from May in Fig. 5). The other
351 methods (TEC-IRI and 6hMAQd) presented high χ-values and therefore were also
352 disregarded.

353 Figure 5 shows the annual variation of dispersion coefficient values calculated for each of
354 the methods. Each color represents the χ-values monthly variation for each non-perturbed
355 reference method during the year 2015 (black: monthly medians, red: TEC-IRI, blue:
356 1hMAQd, orange: 3hMAQd, and green: 6hMAQd), for the three TEC sites (SLZ, SJC,
357 and SMA).

358 From Figure 5, it can be seen that the dispersion coefficient of the 1hMAQd method
359 presented low values ranging from 0 to about 0.2 for all TEC sites, attesting to the good
360 performance of the method. The 3hMAQd method presented dispersion values quite
361 similar to those obtained for the 1hMAQd method, along with the same consistency
362 during the year. The difference between the dispersion coefficients of these methods is
363 0.03, which shows that the use of the 3hMAQd method instead of 1hMAQd in the new
364 DIX calculation is not greatly affected. In respect to the monthly medians, the dispersion
365 coefficient presented inconstant values during January, April, and May, which confirms
366 that this method is strongly influenced by outliers. Moreover, the TEC-IRI and 6hMAQd
367 methods were disregarded because their dispersion coefficient values remained very high
368 throughout the entire period.

369 Thus, the selected method for the determination of the new DIX non-perturbed reference
370 was the one represented by a 3-hour moving average over the TEC obtained during the
371 reference day. Thereafter, we calculate and validate the new DIX calculated from
372 Equation (2) by using the 3hMAQd method during the period around the St. Patrick's
373 Day magnetic storm.

374

375 **4.3 Validation and application in a space weather event**

376 The aim here is to present the ionospheric response during an extreme magnetic storm,
377 discussing the observed differences when applying the proposed method on the Equation
378 (2) and using the original DIX methodology, without giving too much emphasis to the
379 physical explanation for the ionospheric disturbances. Given this context, we have
380 chosen the St. Patrick's Day magnetic storm (17-18 March 2015) to discuss the observed
381 differences in the DIX values obtained from both methodologies. The temporal variations
382 of interplanetary and geophysical parameters during this intense geomagnetic storm are
383 detailed in Astafyeva et al. (2015). Figure 6 shows the new DIX time variation (panel 'a')

384 superposed by the Dst index during the period from 16 to 21 March 2015, at the SJC TEC
385 site. Furthermore, 14 March was chosen to be the reference day for the calculation of the
386 3hMAQd values. The panel 'b' presents the same parameters as on the previous panel,
387 but this time showing the original DIX time variation, where the non-perturbed reference
388 was obtained by the method of the monthly medians. It is important to mention that the
389 original DIX scale ranging from 0 to 2 was chosen to better observe the peaks of the
390 original method and to compare it with the new approach. At last, the panel 'c' presents
391 the time variation for the non-perturbed curves obtained from the 3hMAQd (red curve)
392 and Median (blue curve) methods, as well as the daily TEC variation (gray curve) related
393 to the studied period. Hatched rectangles identified by the numbers from 1 to 4 point out
394 time intervals on which this analysis is focused.

395 Throughout this period of study, the Dst index values remained close to zero on 16
396 March. However, on 17 March the occurrence of an extreme magnetic storm caused the
397 Dst index value to decrease to about -223 nT during the magnetic storm main phase,
398 which lasted until near 00:00 UT on 18 March. It is also noteworthy that this event is
399 known as the St. Patrick's Day magnetic storm and its effects on the ionosphere have

400 been constantly studied (Astafyeva et al., 2015; Wu et al., 2016; Venkatesh et al., 2017;
401 Barbosa et al., 2018). Regarding the time evolution of this space weather event, the storm
402 recovered on 25 March, with Dst index values approaching zero around 13:00 UT
403 (Venkatesh et al., 2017; Maurya et al., 2018).

404 It should be noted that the new DIX detected the occurrence of ionospheric disturbances
405 during almost all the period, while these responses presented some inconsistencies when
406 observed in the original DIX values. For instance, on 16 March around 00:00-09:00 UT
407 we can see that the new DIX presented two periodic peaks ranging between scales 1 and 2
408 (hatched area 1), which is barely observed by the original DIX. These disturbances are
409 strongly associated with the occurrence of Spread F in the pre-storm period (see
410 ionograms in Figure 7). Hence, while the new DIX presented a clear and periodic
411 behavior in detecting the Spread F TEC response, the original DIX presented a noisy
412 behavior, not unlike the one observed throughout the entire daily variation for 16 March.

413

414 On the 17th, during the storm main phase, it can be observed in both DIX methodologies
415 a slight disturbance between 14:00 UT, which extends to 10:00 UT on the 18th. These
416 peaks are directly associated with TEC increases related to the storm-related Prompt
417 Penetration Electric Field (PPEF) occurrence in low latitudes (Venkatesh et al., 2017).
418 Regarding the daytime TEC increases due to PPEF, both indices had a similar response.
419 However, it can be seen that the original DIX tended to overestimate nighttime TEC
420 increases (vertical line '3'), which may be a direct consequence of the original DIX
421 equation, which considers a percentage variation in its calculation. In contrast, the
422 original DIX presented a quite progressive behavior during the PPEF occurrence,
423 gradually increasing its value to the level 5 (extremely disturbed state), and then
424 decreasing until it returned to near zero (quiet state) while the electric field became less
425 effective in disturbing the TEC.

426 Other indications of overestimation in the original DIX nighttime ionospheric response
427 can also be seen on the 19th and 20th (hatched areas 4 and 5, respectively), where the
428 difference between the measured daily TEC and the median-based reference is clearly
429 smaller at night, however, the index shows higher values. The same is not seen in the new

DIX values, which show a response consistent with the difference between the measured daily TEC and the 3hMAQd reference, irrespective of the period of the day.

5 Conclusions

In this paper, we proposed and evaluated a new method to determine the non-perturbed TEC reference for the new DIX as it was described in Denardini et al., (2020a). The conclusions are summarized below:

1. Monthly medians can be highly influenced by TEC values obtained during geomagnetically disturbed days since its dispersion coefficient presented inconstant values in January, April, and May. This behavior confirms that this method is strongly influenced by outliers, and the authors recommend not using such a method.
2. TEC-IRI values tend to be similar to those from the reference day only during the time interval between 00 UT and 12 UT. Moreover, the TEC-IRI method

444 was disregarded because its dispersion coefficient values remained very high
445 throughout the entire period of study.
446 3. All non-perturbed TEC references tend to be more dispersed (concerning the
447 qTEC values) on the site located near the EIA southern crest (SJC).
448 4. The non-perturbed TEC reference method that comes closest to qTEC is the one
449 obtained from the calculation of a 1-hour moving average over the TEC
450 obtained during the reference day (1hMQd). However, the 3hMAQd method is a
451 better way to improve the new DIX sensitivity to short time scale ionospheric
452 phenomena. The difference between the dispersion coefficients of these methods
453 is 0.03, which shows that the use of the 3hMAQd method instead of 1hMAQd in
454 the new DIX calculation is not greatly affected. Also, both methods
455 demonstrated to have stable dispersion coefficients along the whole year of
456 analysis.
457 5. The 3hMAQd method applied to the new DIX calculation showed a better
458 response to magnetic storms than the original DIX, which uses monthly medians.
459 Moreover, it was observed overestimation points in the original DIX nighttime

ionospheric response. The same is not seen in the new DIX values calculated from the proposed non-perturbed reference, which show a coherent ionospheric response irrespective of the period of the day.

Declarations

Ethics approval and consent to participate

Not applicable.

Consent for publication

Not applicable.

List of abbreviations

Availability of data and materials

The data used in the present study are fully open and accessible in acknowledgment basis at the Embrace/INPE Program website (http://www.inpe.br/spaceweather).

Competing interests

The authors declare that they have no competing interests.

Funding

This study was financed in part by the Coordenação de Aperfeiçoamento de Pessoal de Nível Superior - Brasil (CAPES) - Finance Code 001.

Authors' contributions

G. A. S. Picanço conceived the study, designed the data analysis, and leaded writing this manuscript.

C. M. Denardini assisted to conceive the study, design and process the data analysis, as well as to discuss the results of the study.

P. A. B. Nogueira assisted to conceive the study, design and process the data analysis, as well as to discuss the results of the study.

493 P. F. Barbosa Neto performed the GNSS data processing, developed codes for the DIX
494 calculation and some of the data analysis.
495 L. C. A. Resende assisted to design the study and to perform the ionosonde data
496 analysis.
497 C. S. Carmo assisted with the computational codes for data processing and to discuss
498 the results of the study.
499 E. Romero Hernandez developed/adapted the computational codes for GNSS data
500 processing, and assisted to review the manuscript and to discuss the results of the study.
501 S. S. Chen helped with computational codes for data processing and assisted to review
502 the manuscript and to discuss the results of the study.
503 J. Moro assisted to review the manuscript and discuss the results of the study.
504 R. P. Silva assisted to review the manuscript and discuss the results of the study.
505 All the authors helped to write and revise this manuscript.
506

507 Acknowledgements

508 The authors thank the Embrace/INPE Space Weather Program for providing the TEC
509 data, the IBGE for providing the raw TEC data, and the DIDAE/INPE for providing the

ionosonde data to Embrace/INPE. G. A. S. Picanço thanks CNPq/MCTIC (Grant 132252/2017-1) and Capes/MEC (Grant 88887.351778/2019-00). C. M. Denardini thanks CNPq/MCTIC (Grant 303643/2017-0). P. F. Barbosa Neto thanks Capes/MEC (Grant 1622967). L C. A. Resende would like to thank the China-Brazil Joint Laboratory for Space Weather (CBJLSW), National Space Science Center (NSSC), Chinese Academy of Sciences (CAS) for supporting her postdoctoral fellowship. C. S. Carmo thanks CNPq/MCTIC for supporting her Ph.D (Grant 141935/2020-0). S. S. Chen thanks CNPq/MCTIC (Grant 134151/2017-8) and Capes/MEC (Grant 88887.362982/2019-00). J. Moro thanks the China-Brazil Joint Laboratory for Space Weather (CBJLSW), NSSC/CAS for supporting his postdoctoral fellowship, and the National Council for Scientific and Technological Development (CNPq) for the grant 429517/2018-01. R. P. Silva thanks CNPq/MCTIC (Grant 300986/2020-3).

Authors' information

Affiliations

National Institute for Space Research - INPE, Aeronomy Division, São José dos Campos, Brazil

Giorgio Arlan da Silva Picanço, Clezio Marcos Denardini, Paulo França Barbosa Neto, Carolina de Sousa do Carmo & Sony Su Chen

Northeast Regional Center – CRN/INPE, Natal, Brazil

Régia Pereira da Silva

National Space Science Center, China Academy of Science – NSSC/CAS, Beijing, China

Láysa Cristina Araújo Resende & Juliano Moro

Federal Institute of Education, Science and Technology of São Paulo - IFSP, Jacareí, Brazil

Paulo Alexandre Bronzato Nogueira

Universidad Autónoma de Nuevo León, Facultad de Ciencias Físico-Matemáticas – UANL/FCFM, Monterrey, Mexico

Esmeralda Romero Hernández

References

Abdu, M. A. (2005), Equatorial ionosphere–thermosphere system: electrodynamics and irregularities, Advances in Space Research, 35, 771–787, doi:10.1016/j.asr.2005.03.150.

Abdu, M. A., de Souza, J. R., Sobral, J. H. A., and Batista, I. S. (2006), Magnetic storm associated disturbance dynamo effects in the low and equatorial latitude ionosphere, Geophysical Monograph Series, 167, 283–304, doi:10.1029/167GM22.

Abdu, M. A., Batista, I. S., Reinisch, B., de Souza, J., Sobral, J. H. A., Pedersen, T., Medeiros, A., Schuch, N., de Paula, E., Groves, K. (2009), Conjugate Point Equatorial

549 Experiment (COPEX) Campaign in Brazil: Electrodynamics highlights on spread F
550 development conditions and day-to-day variability, Journal of Geophysical Research:
551 Space Physics, 114(4), doi:10.1029/2008JA013749.

552 Astafyeva, E., Zakharenkova, I., and Förster, M. (2015), Ionospheric response to the
553 2015 St. Patrick's Day storm: a global multi-instrumental overview, Journal of
554 Geophysical Research, 120, 9023–9037, doi:10.1002/2015JA021629.

555 Barbosa, F. R. E., Fagundes, P. R., Venkatesh, K., Fejer, B. G, Pillat, V. G., Denardini, C.
556 M., Muella, M. T. A. H. (2018), Multi-scale ionospheric irregularities occurrence over
557 South America during the St. Patrick's day storm on March 17, 2015, Journal of
558 Atmospheric and Solar-Terrestrial Physics, 174, 32-45, doi:10.1016/j.jastp.2018.05.001.

559 Batista, I. S., de Paula, E. R., Abdu, M. A., Trivedi, N. B., and Greenspan, M. E. (1991),
560 Ionospheric effects of the March 13, 1989, magnetic storm at low and equatorial
561 latitudes, Journal of Geophysical Research: Space Physics, 96(A8), 13943–13952.
562 doi:10.1029/91ja01263.

563 Bilitza, D., Altadill, D., Truhlik, V., Shubin, V., Galkin, I., Reinisch, B., and Huang, X.
564 (2017), International Reference Ionosphere 2016: From ionospheric climate to real-time
565 weather predictions, Space Weather, 15(2), 418–429, doi:10.1002/2016SW001593.

566 Blanc, M., and Richmond, A. D. (1980), The ionospheric disturbance dynamo, Journal
567 of Geophysical Research, 85, 1669-1669, doi:10.1029/JA085iA04p01669.

568 Denardini, C. M., Picanço, G. A. S., Barbosa Neto, P. F., Nogueira, P. A. B., Carmo, C.
569 S., Resende, L. C. A., Moro, J., Chen, S. S., Romero-Hernandez, E., Silva, R. P., and
570 Bilibio, A. V. (2020a), Ionospheric Scale Index Map Based on TEC Data for Space
571 Weather Studies and Applications, Space Weather, Accepted manuscript
572 2019SW002328RRR.

573 Denardini, C. M., Picanço, G. A. S., Barbosa Neto, P. F., Nogueira, P. A. B., Carmo, C.
574 S., Resende, L. C. A., Moro, J., Chen, S. S., and Bilibio, A. V. (2020b),), Ionospheric
575 Scale Index Map Based on TEC Data during the Saint Patrick Magnetic Storms and
576 EPBs, Space Weather, Accepted manuscript 2019SW002330RRR.

577 de Siqueira, P. M., de Paula, E. R., Muella, M. T. A. H., Rezende, L. F. C., Abdu, M. A.,
578 and Gonzalez, W. D. (2011), Storm-time total electron content and its response to
579 penetration electric fields over South America, Annales Geophysicae, 29, 1765–1778,
580 doi:10.5194/angeo-29-1765-2011.

581 Figueiredo, C. A. O. B., Wrasse, C. M., Takahashi, T., Otsuka, Y., Shiokawa, K., and
582 Barros, D. (2017), Large-scale traveling ionospheric disturbances observed by GPS
583 dTEC maps over North and South America on Saint Patrick's Day storm in 2015,
584 Journal of Geophysical Research: Space Physics, 122, 4755–4763,
585 doi:10.1002/2016JA023417.

586 Figueiredo, C. A. O. B., Takahashi, H., Wrasse, C. M., Otsuka, Y., Shiokawa, K., and
587 Barros, D. (2018a), Medium-scale traveling ionospheric disturbances observed by

588 detrended total electron content maps over Brazil, Journal of Geophysical Research:
589 Space Physics, 123, 2215–2227, doi:10.1002/2017JA025021.

590 Figueiredo, C. A. O. B., Takahashi, H., Wrasse, C. M., Otsuka, Y., Shiokawa, K., and
591 Barros, D. (2018b), Investigation of nighttime MSTIDS observed by optical
592 thermosphere imagers at low latitudes: Morphology, propagation direction, and wind
593 filtering, Journal of Geophysical Research: Space Physics, 123, 7843–7857,
594 doi:10.1029/2018JA025438.

595 Gulyaeva, T. L., and Stanislawska, I. (2008), Derivation of a planetary ionospheric
596 storm index, Annales Geophysicae, 26(9), 2645-2648,
597 doi:10.5194/angeo-26-2645-2008.

598 Jakowski, N., Stankov, S. M., Schlueter, S., and Klaehn, D. (2006), On developing a
599 new ionospheric perturbation index for space weather operations, Advances in Space
600 Research, 38, 2596-2600, doi:10.1016/j.asr.2005.07.043.

601 Jakowski, N., Béniguel, Y., De Franceschi, G., Pajares, M. H., Jacobsen, K. S.,
602 Stanislawska, I., Tomasik, L., Warnant, R., and Wautelet, G. (2012a), Monitoring,
603 tracking and forecasting ionospheric perturbations using GNSS techniques, Journal of
604 Space Weather and Space Climate, 2, doi:10.1051/swsc/2012022.

605 Jakowski, N., Borries, C., and Wilken, V. (2012b), Introducing a disturbance ionosphere
606 index, Radio Science, 47(3), doi:10.1029/2011RS004939.

607 Jakowski, N., and Hoque, M. M. (2019), Estimation of spatial gradients and temporal
608 variations of the total electron content using ground-based GNSS measurements, Space
609 Weather, 17, 339–356, doi:10.1029/2018SW002119.

610 Kelley, M. C., Fejer, B. G., and Gonzales, C. A. (1979), An explanation for anomalous
611 ionospheric electric fields associated with a northward turning of the interplanetary
612 magnetic field, Geophysical Research Letters, 6, 301–304,
613 doi:10.1029/GL006i004p00301.

614 Klobuchar, J. A. (1991), Ionospheric effects on GPS, GPS World, 2(4), 48–51.

615 Maurya, A. K., Venkatesh, K., Kumar, S., Singh, R., Tiwari, P., Singh, A. K. (2018),
616 Effects of St. Patrick's day geomagnetic storm of March 2015 and of June 2015 on
617 low-Equatorial D region ionosphere, Journal of Geophysical Research, 123, 6836–6850,
618 doi: 10.1029/2018JA025536l.

619 Nogueira, P. A. B., Abdu, M. A., Batista, I. S., and de Siqueira, P.M. (2011), Equatorial
620 ionization anomaly and thermospheric meridional winds during two major storms over
621 Brazilian low latitudes, Journal of Atmospheric and Solar-Terrestrial Physics, 73,
622 1535-1543, doi: 10.1016/j.jastp.2011.02.008.

623 Otsuka, Y., Ogawa, T., Saito, A., Tsugawa, T., Fukao, S., Miyazaki, S. (2002), A new
624 technique for mapping of total electron content using GPS network in Japan, Earth
625 Planets Space, 54, 63–70, doi: 10.1186/BF03352422.

626 Resende, L. C. A., Denardini, C. M., Picanço, G. A. S., Moro, J., Barros, D., Figueiredo,
627 C. A. O. B., and Silva, R. P. (2019). On developing a new ionospheric plasma index for
628 the Brazilian equatorial F region irregularities. Annales Geophysicae, 37, 807–818, doi:
629 10.5194/angeo-37-807-2019.

630 Sanz, J., Juan, J. M., González-Casado, G., Prieto-Cerdeira, R., Schlüter, S., Orús, R.
631 (2014), Novel Ionospheric Activity Indicator Specifically Tailored for GNSS Users,
632 Proceedings of the 27th International Technical Meeting of the Satellite Division of The
633 Institute of Navigation (ION GNSS+ 2014), Tampa, Florida, September 2014,
634 1173-1182.

635 Shinbori, A., Otsuka, Y., Tsugawa, T., Nishioka, M., Kumamoto, A., Tsuchiya, F.,
636 Matsuda, S., Kasahara, Y., Matsuoka, A., Ruohoniemi, J. M., Shepherd, S. G., and
637 Nishitani, N. (2018), Temporal and spatial variations of storm time midlatitude
638 ionospheric trough based on global GNSS-TEC and Arase satellite observations,
639 Geophysical Research Letters, 45, 7362–7370, doi:10.1029/2018GL078723.

640 Sobral, J. H. A., Abdu, M. A., Gonzalez, W. D., Tsuturani, B. T., Batista, I. S., and
641 Gonzalez, A. L. (1997), Effects of intense storms and substorms on the equatorial
642 ionosphere/thermosphere system in the American sector from ground-based and satellite
643 data, Journal of Geophysical Research: Space Physics, doi:10.1029/97JA00576.

644 Takahashi, H., Costa, S., Otsuka, Y., Shiokawa, K., Monico, J. F. G., Paula, E., Nogueira,
645 P., Denardini, C. M., Becker-Guedes, F., Wrasse, C. M., Ivo, A. S., Gomes, V. C. F.,

646 Gargarela, W., Sant'Anna, N., and Gatto, R. (2014), Diagnostics of equatorial and low
647 latitude ionosphere by TEC mapping over Brazil, Advances in Space Research, 54(3),
648 385-394, doi: 10.1016/j.asr.2014.01.032.

649 Takahashi, H., Wrasse, C. M., Denardini, C. M., Pádua, M. B., de Paula, E. R., Costa, S.
650 M. A., Otsuka, Y., Shiokawa, K., Galera Monico, J. F., Ivo, A., and Sant'Anna, N.
651 (2016), Ionospheric TEC Weather Map Over South America, Space Weather, 14(11),
652 937–949, doi:10.1002/2016SW001474.

653 Takahashi, H., Wrasse, C. M., Figueiredo, C. A. O. B., Barros, D., Abdu, M. A., Otsuka,
654 Y., and Shiokawa, K. (2018), Equatorial plasma bubble seeding by MSTIDs in the
655 ionosphere, Progress in Earth and Planetary Science, 5:32,
656 doi:10.1186/s40645-018-0189-2.

657 Tsugawa, T., Nishioka, M., Ishii, M., Hozumi, K., Saito, S., Shinbori, A., Otsuka, Y.,
658 Saito, A., Buhari, S., Abdullah, M. and Supnithi, P. (2018), Total Electron Content
659 Observations by Dense Regional and Worldwide International Networks of GNSS,
660 Journal of Disaster Research, 13(3), 535-545, doi: 10.20965/jdr.2018.p0535.

661 Venkatesh, K.; Tulasi Ram, S.; Fagundes, P. R.; Seemala, G. K.; Batista, I. S.
662 Electrodynamic disturbances in the Brazilian equatorial and low-latitude ionosphere on
663 St. Patrick's Day storm of 17 March 2015. Journal of Geophysical Research: Space
664 Physics, v. 122, p. 4553–4570, 2017.

665 Voeykov, S. V., Yasyukevich, A. S., Edemskiy, I. K., Perevalova, N. P., and Yasyukevich,

666 Y. V. (2018), WTEC: A new index to estimate the intensity of ionospheric disturbances,
667 Results in Physics, 11, 1056–1057, doi:10.1016/j.rinp.2018.11.023.

668 Wilken, V., Kriegel, M., Jakowski, N., and Berdermann, J. (2018), An ionospheric index
669 suitable for estimating the degree of ionospheric perturbations, Journal of Space
670 Weather and Space Climate, 8(A19), doi:10.1051/swsc/2018008.

671 Wu, C. C., Fry, C. D., Liu, J. Y., Liou, K., and Tseng, C. L. (2004), Annual TEC
672 variation in the equatorial anomaly region during the solar minimum: September 1996–
673 August 1997, Journal of Atmospheric and Solar-Terrestrial Physics, 66, 199–207, doi:
674 10.1016/j.jastp.2003.09.017.

675 Wu, C., Liou, K., Lepping, R., Hutting, L., Plunkett, S., Howard, R., and Socker, D.
676 (2016), The first super geomagnetic storm of solar cycle 24: "The St. Patrick's day
677 event (17 March 2015)", Earth, Planets and Space, 68(1),
678 doi:10.1186/s40623-016-0525-y.

679

680

681

682

683

684

685

686 **Figure captions**

687 **Figure 1 -** Sequence of ionograms from 21:00 UT to 22:20 UT on March 14, 2015,
688 demonstrating the absence of spread-F over Cachoeira Paulista.

689 **Figure 2** - TEC map on 14 March, 2015 showing the geographic locations of the three
690 TEC single-points used in this study: SLZ, SJC, SMS.

691 **Figure 3** - Time variation of non-perturbed TEC references calculated from each of the
692 methods (black lines: monthly medians, red lines: TEC-IRI, blue lines: 1hMAQd,
693 orange lines: 3hMAQd, and green lines: 6hMAQd), for the three TEC sites (SLZ, SJC,
694 and SMA) on February 2015, from the TEC measurements (gray lines).

695 **Figure 4** - Scatter plots of the non-perturbed references calculated from the monthly
696 medians (black symbols), TEC-IRI (red symbols), 1hMAQd (blue symbols), 3hMAQd
697 (orange symbols), and 6hMAQd (green symbols) at (a) SLZ, (b) SJC , and (c) SMA
698 against the qTEC values in March 2015, respectively.

699 **Figure 5** - Annual variation of dispersion coefficient values related to the monthly
700 medians (black squares), TEC-IRI (red cyrcles), 1hMAQd (blue diamonds), 3hMAQd
701 (orange hexagons), and 6hMAQd (green stars) at (a) SLZ, (b) SJC, and (c) SMA during
702 the year 2015.

703 **Figure 6** - Time variation of (panel ‘a’) new DIX and (panel ‘b’) original DIX,
704 superposed by the Dst index, and non-perturbed references (panel ‘c’) used for their
705 calculation along with the daily TEC during the period around the St. Patrick’s Day
706 magnetic storm.

707 **Figure 7 -** Sequence of ionograms from 01:30 UT to 02:50 UT on March 16, 2015,

demonstrating the presence of spread-F over Cachoeira Paulista (same SJC observation point). Black arrows indicate spread of the signal.

730 **Table captions**

731 **Table 1** - Geographic and geomagnetic coordinates of the three locations used in this
732 study.

733 **Table 2** - Annual average of dispersion coefficient values obtained for each
734 non-perturbed reference method at the three TEC sites, for the year 2015.

735

736

737

738

739

740

741

742

743

744

745

746

747

748

749

750

751

752 **Figure 1 -**

753

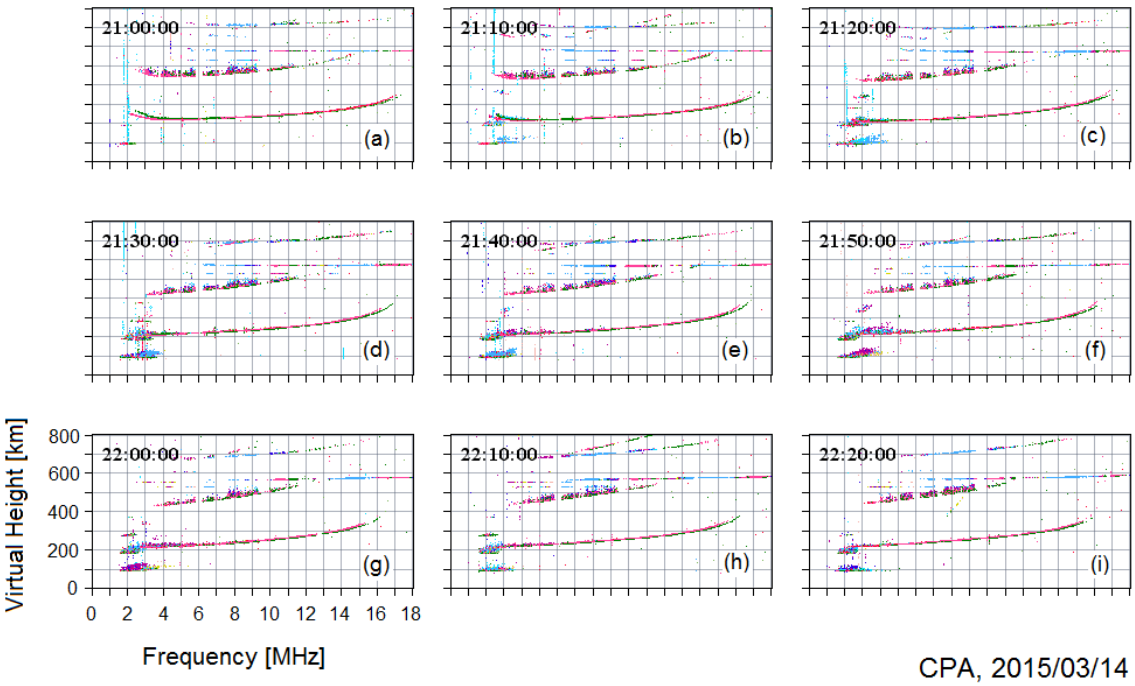

754

755

756

757

758

759

760

761

762

763

764

765

766 **Figure 2 -**

767

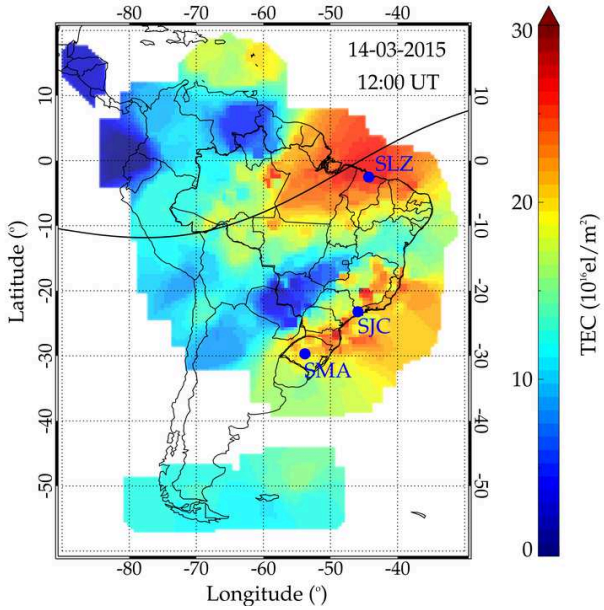

768

769

770

771

772

773

774

775

776

777

778

779

780

781 **Figure 3 –**

782

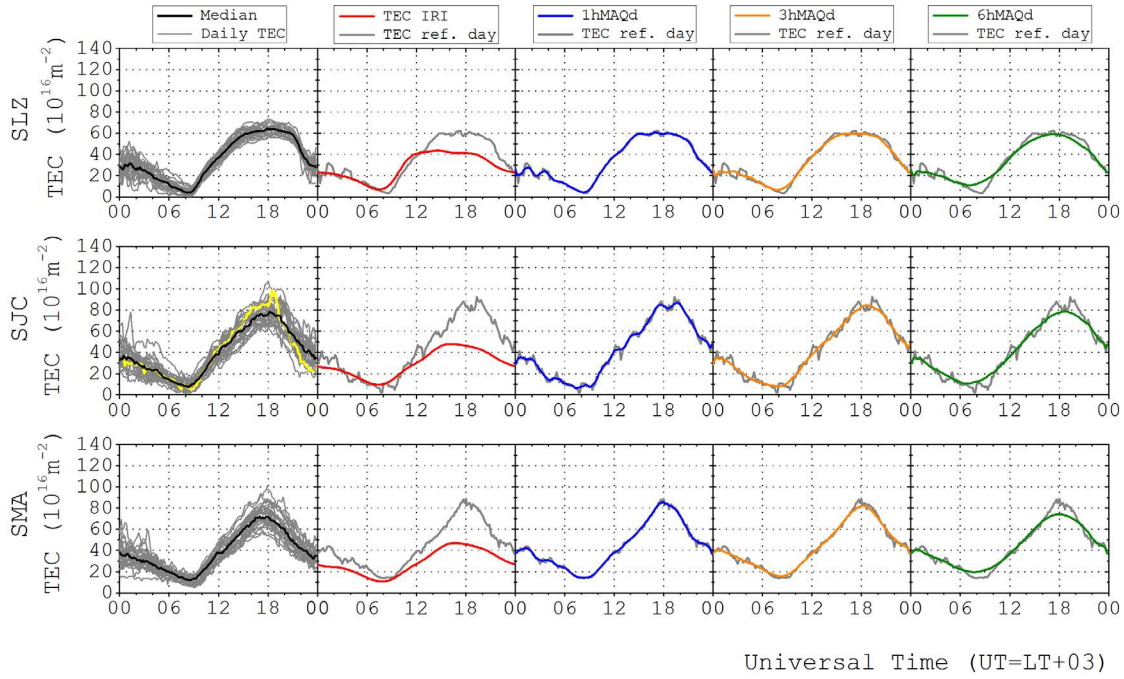

783

784

785

786

787

788

789

790

791

792

793

794

795 **Figure 4 –**

796

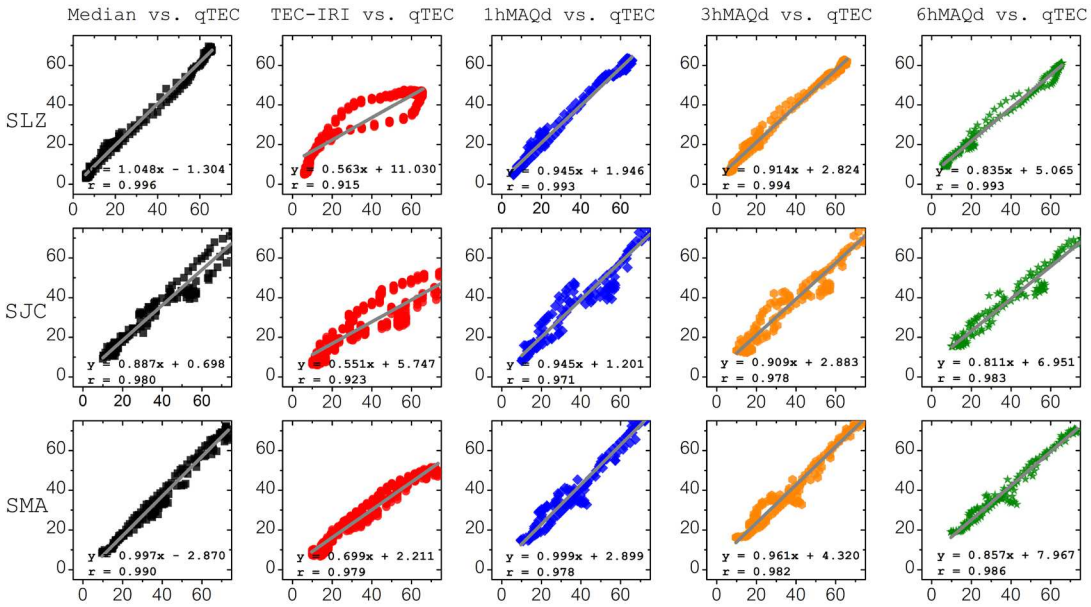

797

798

799

800

801

802

803

804

805

806

807

808

809

Figure 5 –

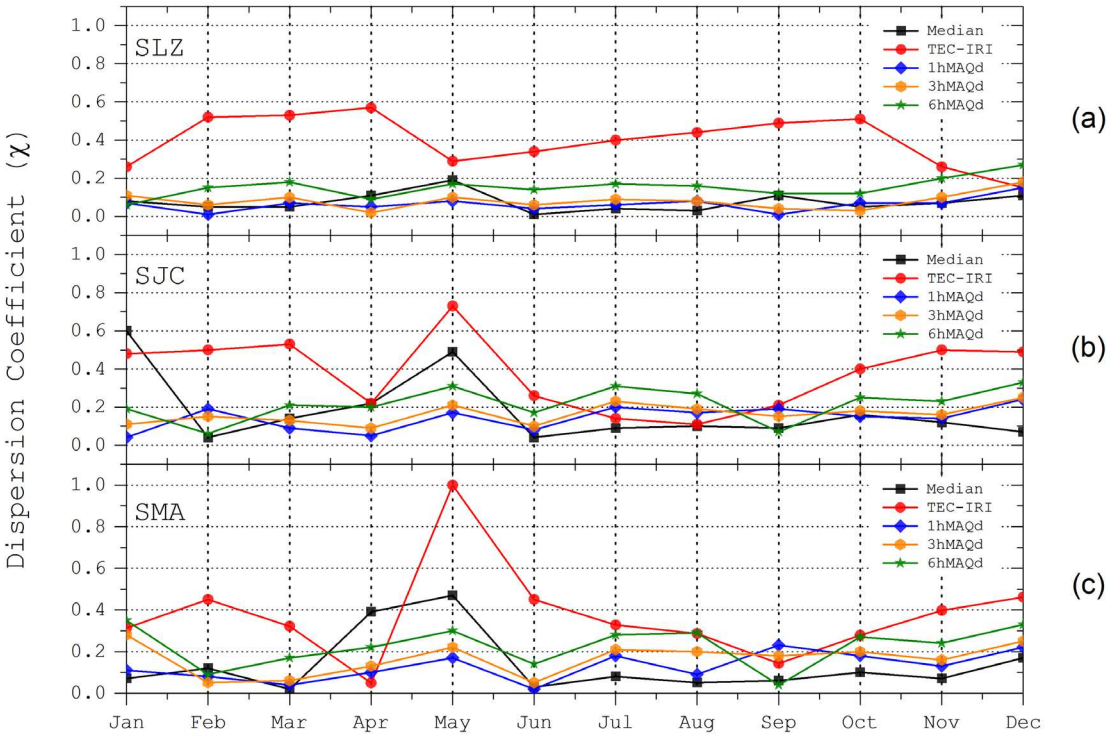
Dispersion Coefficient (χ)
SLZ
SJC
SMA
Median
TEC-IRI
1hMAQd
3hMAQd
6hMAQd
(a)
(b)
(c)
1.0
0.8
0.6
0.4
0.2
0.0
Jan
Feb
Mar
Apr
May
Jun
Jul
Aug
Sep
Oct
Nov
Dec

823 **Figure 6 –**

824

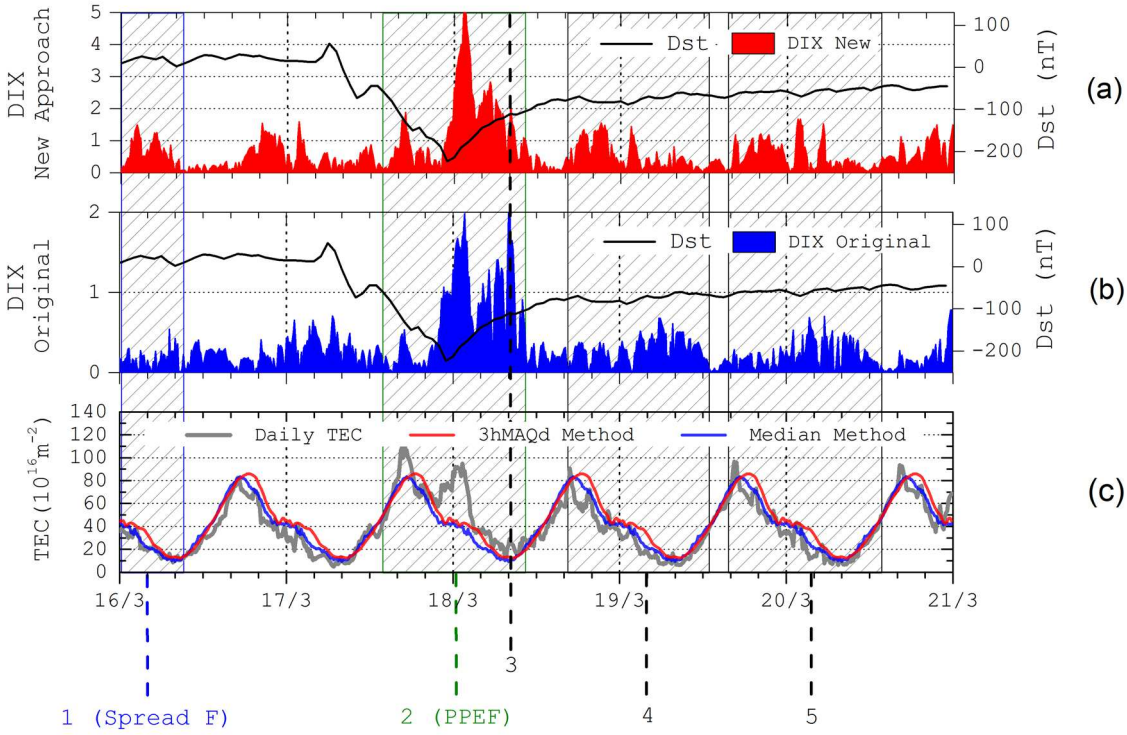

825

826

827

828

829

830

831

832

833

834

835 **Figure 7 –**

836

837

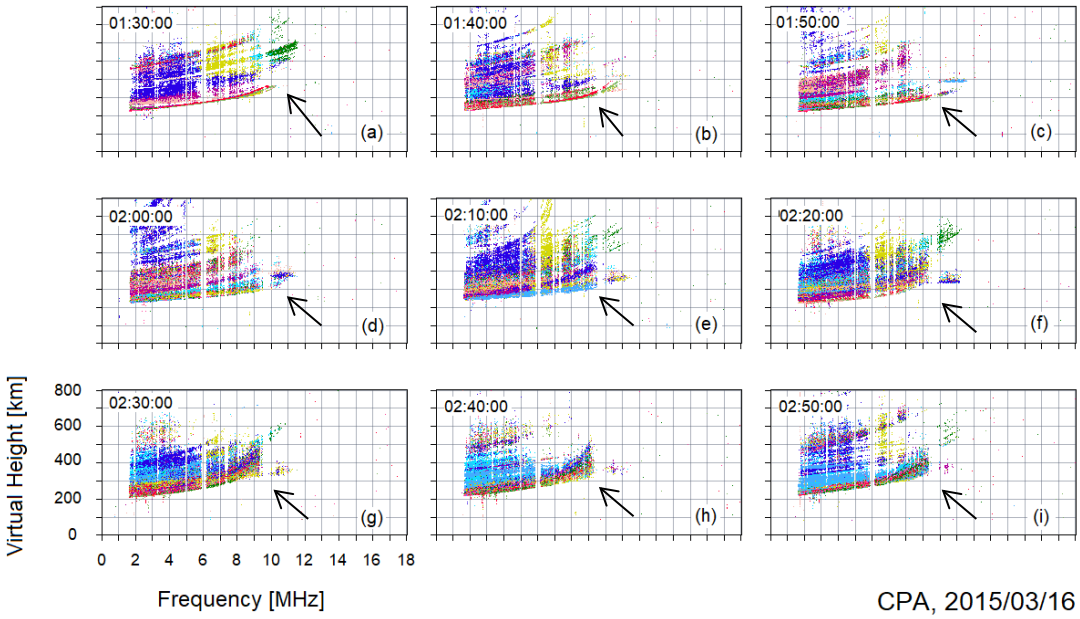

838

839

840

841

842

843

844

845

846

847

848

849

850 **Table 1 –**

851

Location	Geographic Coordinates		Geomagnetic Coordinates	
	Lat.	Lon.	Lat.	Lon.
São Luís (SLZ)	-2.53	-44.30	-3.79	27.03
São José dos Campos (SJC)	-23.17	-45.88	-19.73	20.04
Santa Maria (SMA)	-29.69	-53.80	-21.52	12.83

852

853

854

855

856

857

858

859

860

861

862

863

864

865

866

867 **Table 2 –**

868

	Dispersion Coefficient (χ) – Annual Average				
Location	Median	TEC-IRI	1hMAQd	3hMAQd	6hMAQd
SLZ	0.08	0.40	0.06	0.08	0.15
SJC	0.18	0.38	0.14	0.16	0.22
SMA	0.14	0.39	0.13	0.17	0.23

869

Figures

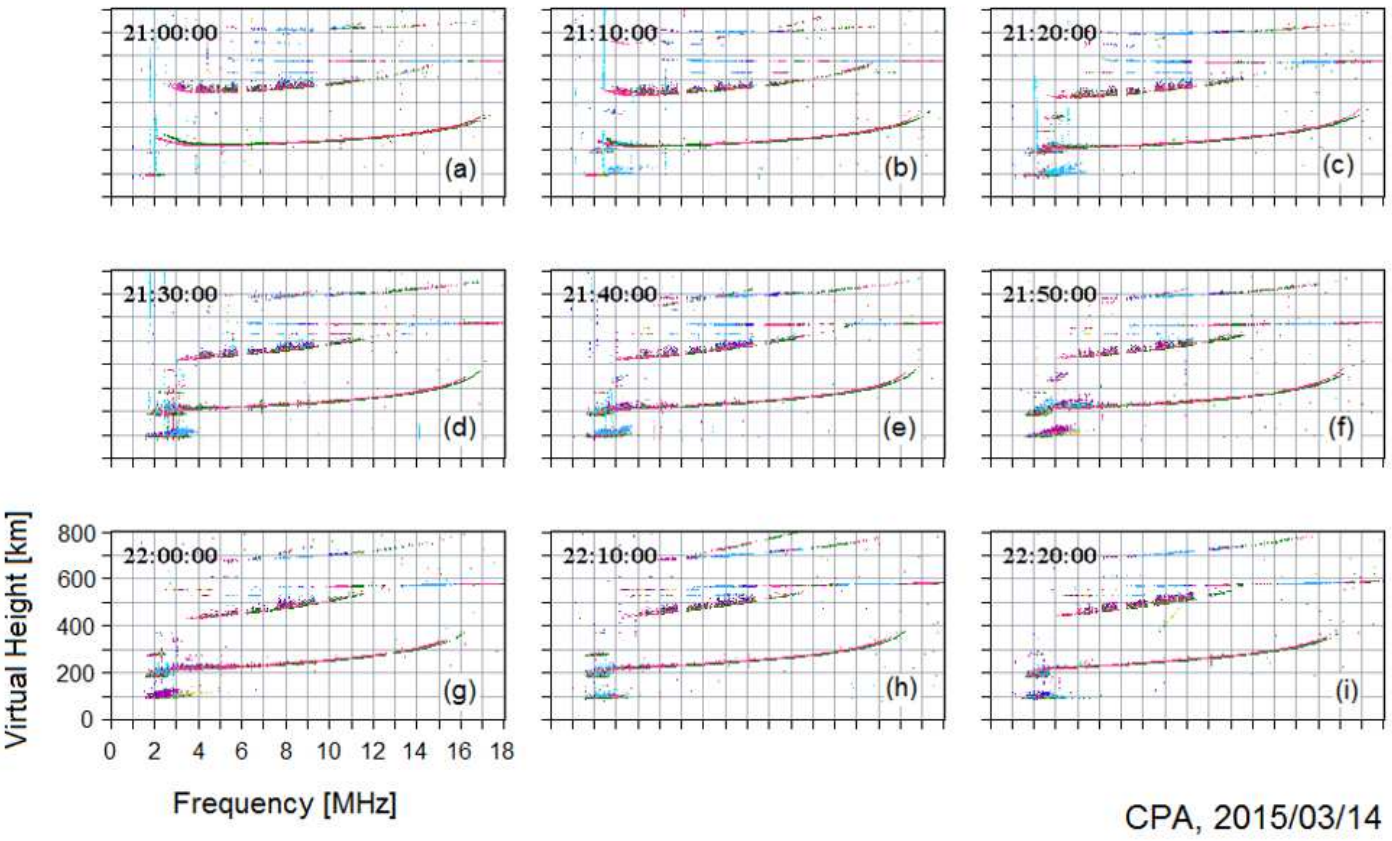

Figure 1

Sequence of ionograms from 21:00 UT to 22:20 UT on March 14, 2015, demonstrating the absence of spread-F over Cachoeira Paulista.

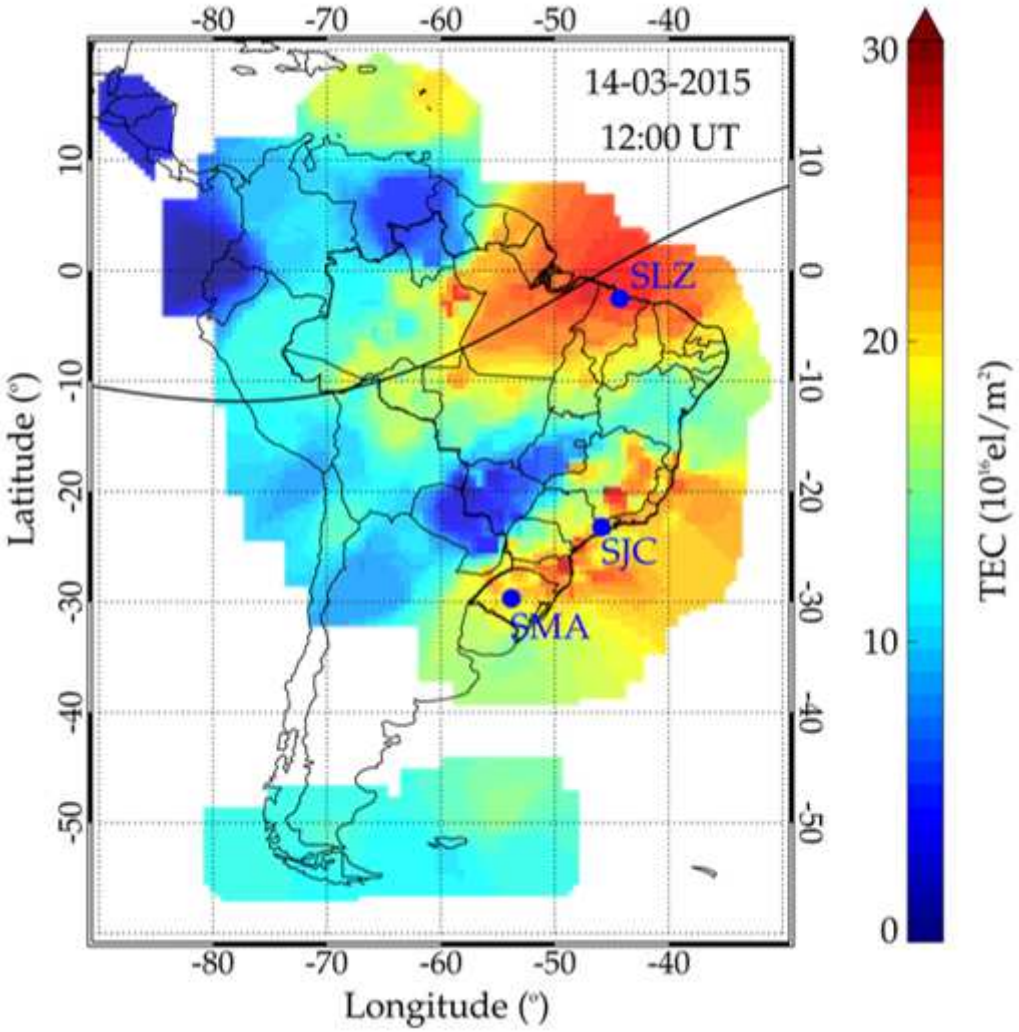

Figure 2

TEC map on 14 March, 2015 showing the geographic locations of the three TEC single-points used in this study: SLZ, SJC, SMS.

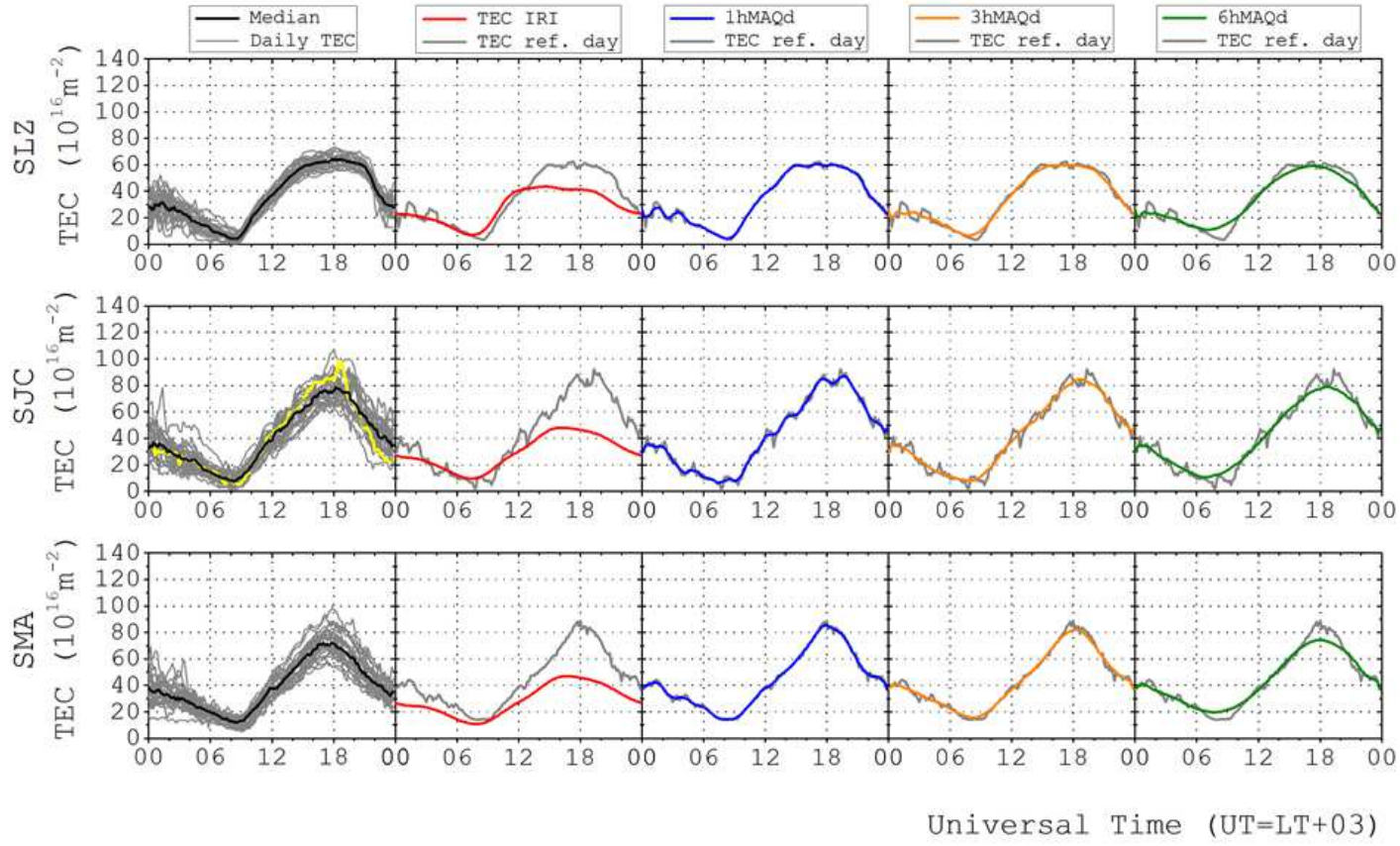

Figure 3

Time variation of non-perturbed TEC references calculated from each of the methods (black lines: monthly medians, red lines: TEC-IRI, blue lines: 1hMAQd, orange lines: 3hMAQd, and green lines: 6hMAQd), for the three TEC sites (SLZ, SJC, and SMA) on February 2015, from the TEC measurements (gray lines).

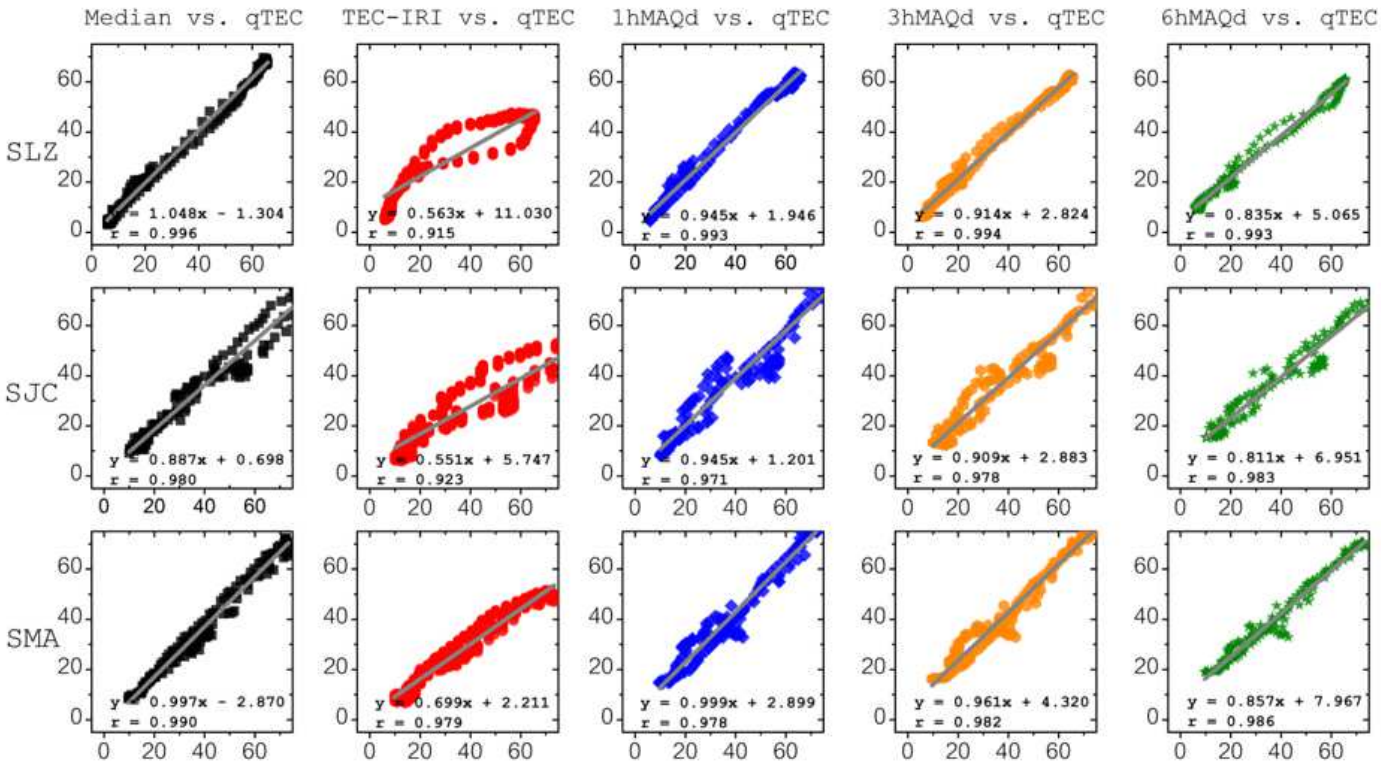

Figure 4

Scatter plots of the non-perturbed references calculated from the monthly medians (black symbols), TEC-IRI (red symbols), 1hMAQd (blue symbols), 3hMAQd (orange symbols), and 6hMAQd (green symbols) at (a) SLZ, (b) SJC , and (c) SMA against the qTEC values in March 2015, respectively.

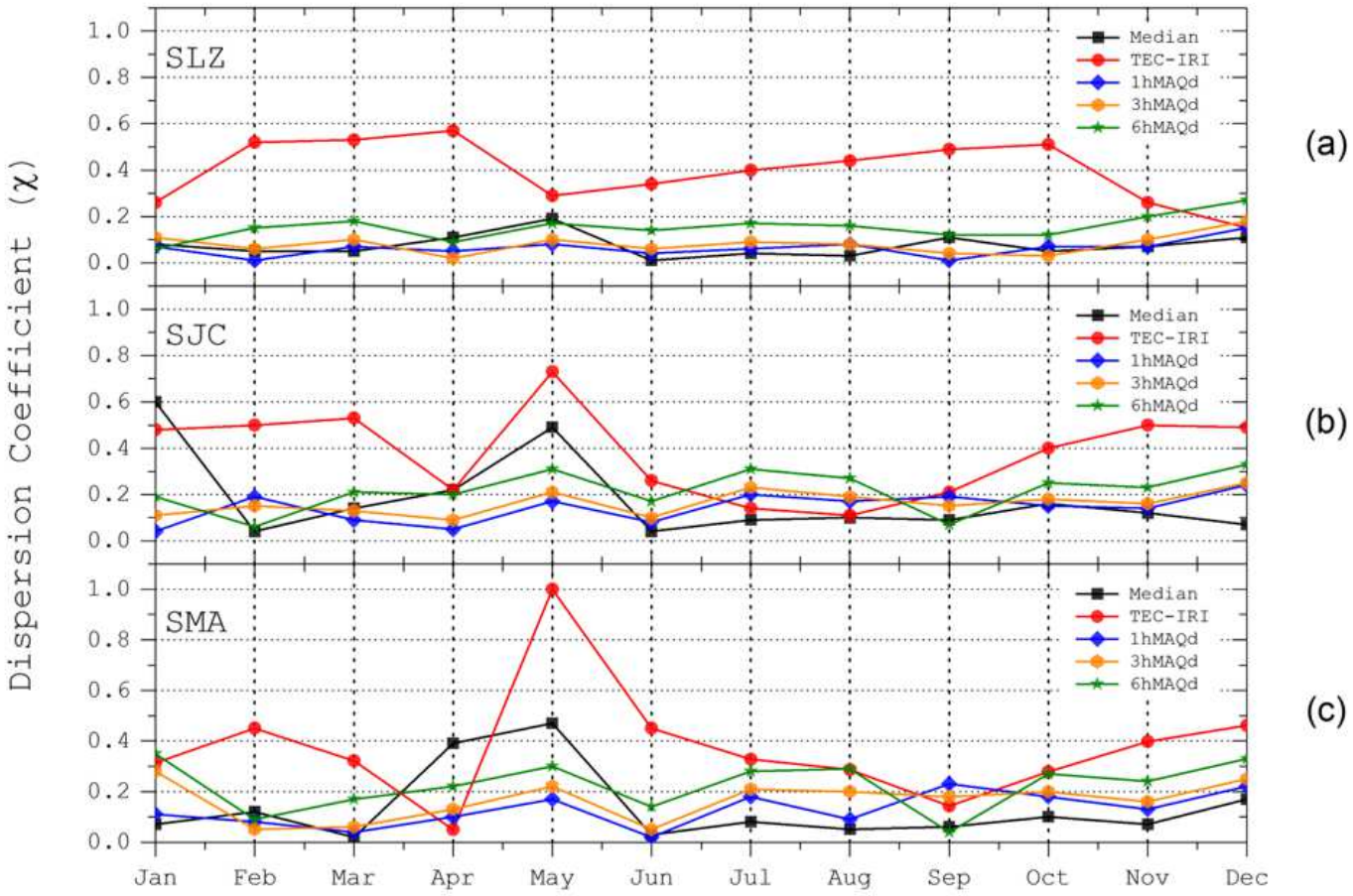

Figure 5

Annual variation of dispersion coefficient values related to the monthly medians (black squares), TEC-IRI (red cyrcles), 1hMAQd (blue diamonds), 3hMAQd (orange hexagons), and 6hMAQd (green stars) at (a) SLZ, (b) SJC, and (c) SMA during the year 2015.

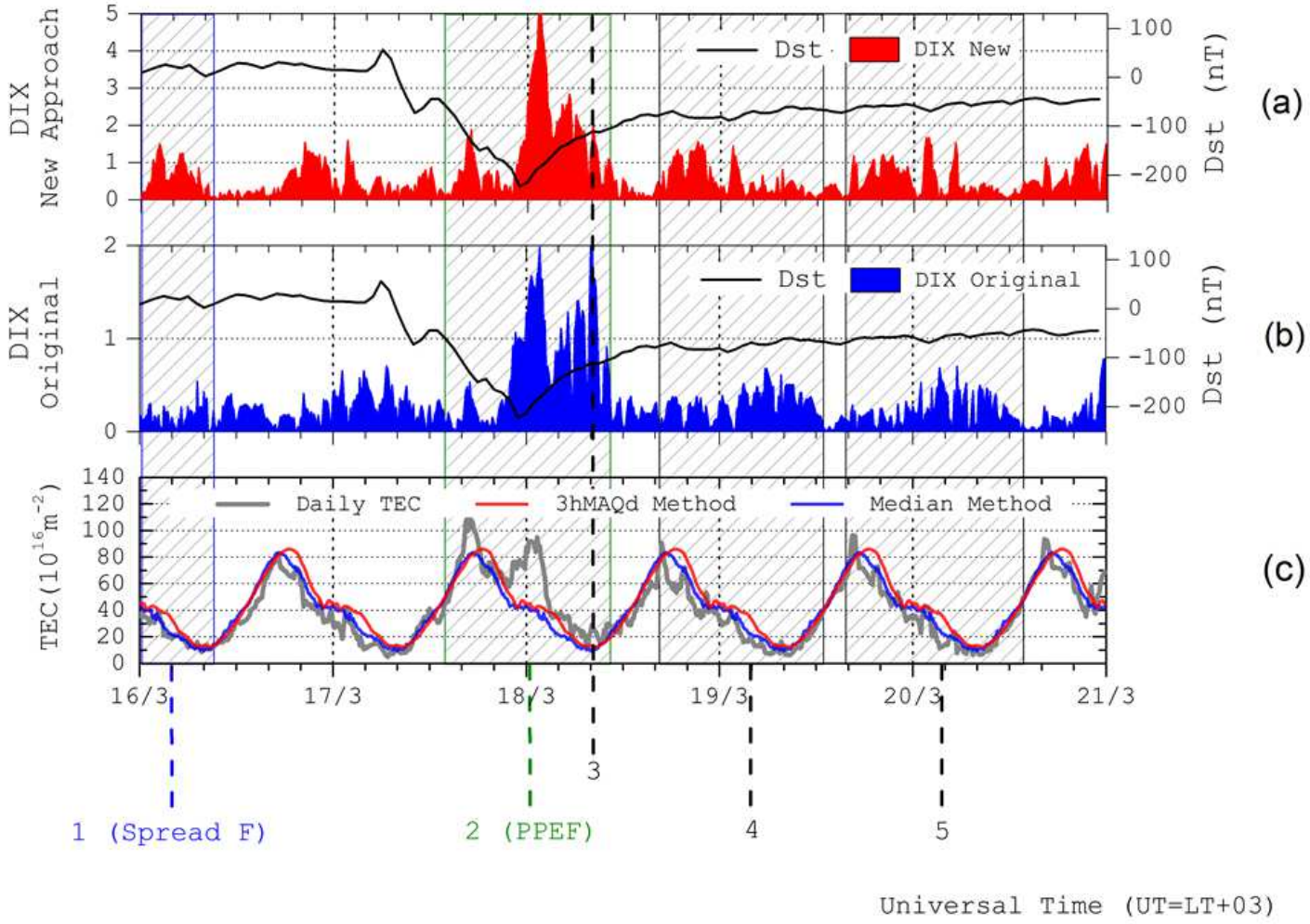

Figure 6

Time variation of (panel ‘a’) new DIX and (panel ‘b’) original DIX, superposed by the Dst index, and non-perturbed references (panel ‘c’) used for their calculation along with the daily TEC during the period around the St. Patrick’s Day magnetic storm.

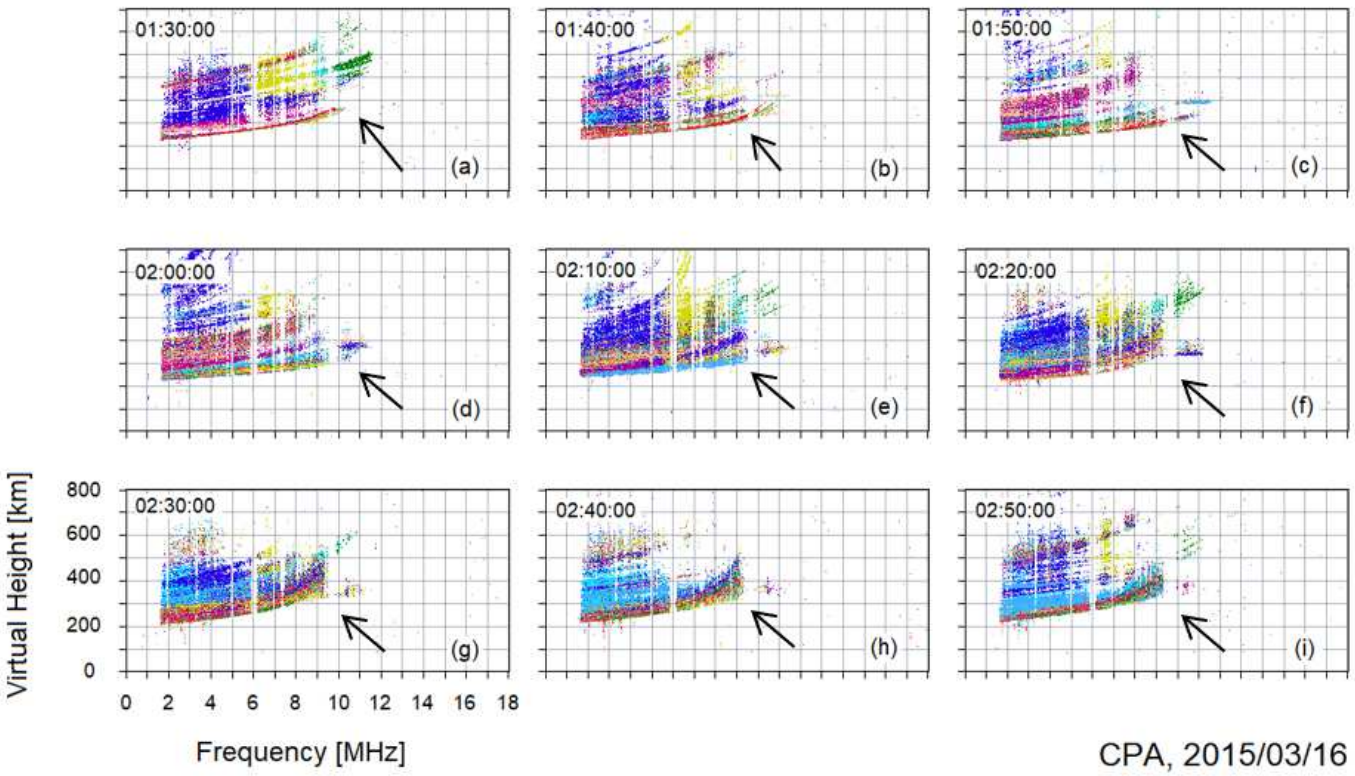

Figure 7

Sequence of ionograms from 01:30 UT to 02:50 UT on March 16, 2015, demonstrating the presence of spread-F over Cachoeira Paulista (same SJC observation point). Black arrows indicate spread of the signal.

Supplementary Files

This is a list of supplementary files associated with this preprint. Click to download.

- graphicalabstractimage.jpg